THE JOURNAL OF PHYSICAL CHEMISTRY LETTERS
A JOURNAL OF THE AMERICAN CHEMICAL SOCIETY

pubs.acs.org/JPCL Letter

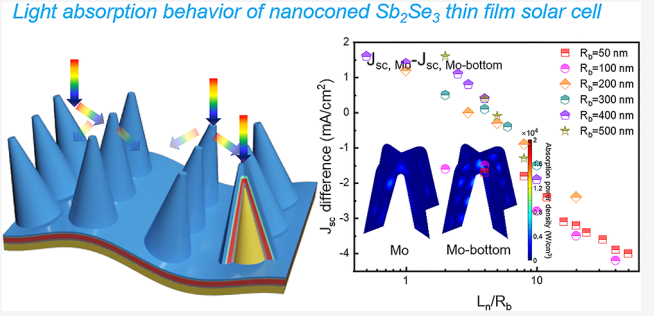
Management of Light Absorption Based on Sidewall Reflection for Fabricating High-Performance Flexible Nano-Coned Sb_2Se_3 Thin Film Photovoltaics

Shaobo Zhang,* Cheng Chen, Yunqing Cao, Xiangdong Meng, Ruijin Hu,* Zongguang Liu, Haifeng Gao, Xiulin Jiang, Junzhuan Wang, and Linwei Yu*

Cite This: *J. Phys. Chem. Lett.* 2024, 15, 9548−9556 Read Online

ACCESS | Metrics & More | Article Recommendations | Supporting Information

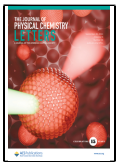
ABSTRACT: High performance and robustness are the key factors to boosting wearable and portable applications. Although the 1D crystal structure makes the Sb_2Se_3 thin film more tolerant to physical deformation upon bending, the conventional planar structures still cannot undergo repeated mechanical bending due to the induced stress/strain inside devices, which can be well addressed by constructing three-dimensional nanostructures. Besides, the electron diffusion length has two values, 0.3 μm in the [221] direction and 1.7 μm in the [001] direction, in the Sb_2Se_3 thin film, which limits the absorber thickness, for getting an effective carrier collection; thus, a strong light trapping effect enabling sufficient light harvesting is needed to allow the use of a very thin light absorption layer. Herein, the nanoconed Sb_2Se_3 solar cells have been designed, and their light absorption behaviors were investigated within a finite-element simulation under the substrate back-reflection, indicating that the reflection of the bottom part always works positively, while the effect of the nanocone sidewall on absorption enhancement largely depends on its geometry, arising from resonant or scattering modes. These results provide a practical guide in designing/establishing an easier/simpler way to fabricate high-performance and mechanically stable flexible nanostructured Sb_2Se_3 thin film solar cells.



How to fabricate both high-performance and mechanically stable thin film solar cells with a high power-to-weight ratio on flexible and lightweight substrates is an important and interesting issue, to meet the increasing demands of wearable and portable applications.[1−6] The antimony selenide (Sb_2Se_3) as a new but promising candidate, has attracted numerous interests for its nontoxicity, abundant reserves, low cost, proper bandgap (E_g) of 1.0−1.3 eV, and a high absorption coefficient of 10^5 cm^{-1}, in fabricating the high-performance and robust flexible thin film solar cells.[7−12] Recently, a champion/recorded power conversion efficiency (PCE) > 10% has been demonstrated on the Mo-coated glass substrates, by preparing high-quality [00*l*]-oriented Sb_2Se_3 thin films as the light absorption layer.[13] Meanwhile, a flexible Sb_2Se_3 thin film solar cell has been demonstrated using a multilayer structure of PI/Mo/Sb_2Se_3/CdS/ZnO/aluminum-doped ZnO (AZO)/Ag, getting a PCE of 8.43%.[14]

Although the unique 1D crystal structure makes the Sb_2Se_3 thin film more tolerant to physical deformation upon bending,[3,15] the planar-structured device still cannot undergo repeated mechanical bending with a small radius; for example, a 6.6% PCE decline was reported for the planar Sb_2Se_3 thin film devices on the SU-8 substrates after 1000 cycles of mechanical bending.[16] Thus, how to more efficiently release the stress and strain inside a photovoltaic device induced by repeated bending is a fundamental issue to improve mechanical stability. Besides, the Sb_2Se_3 thin film usually has two kinds of electron diffusion length (L_e), 1.7 μm in the [001] direction and 0.3 μm in the [221] direction,[17] which is a limitation to the Sb_2Se_3 absorber thickness in the range of 0.3−0.6 μm for an effective carrier collection to fabricate high-efficiency thin film solar cells. However, such thickness of the light absorption layer cannot enable sufficient light harvesting to generate a large enough photocurrent.[17] Thus, how to decouple incident light absorption and photogenerated carrier collection in this thin film absorption layer, for seeking better performance, is an essential issue too. As known, constructing three-dimensional (3D) nanostructures, such as nanocones, nanowires, and so on, has been proven as a beneficial way to improve the flexibility and mechanical stability, compared to the conventional planar

Received: August 17, 2024
Revised: September 8, 2024
Accepted: September 10, 2024
Published: September 12, 2024



Downloaded from pubs.acs.org/jpclcd/article-pdf/15/38/9548/3360106/jz4c02414.pdf by NANJING UNIV user on 04 November 2026

ACS Publications © 2024 American Chemical Society

https://doi.org/10.1021/acs.jpclett.4c02414
J. Phys. Chem. Lett. 2024, 15, 9548−9556

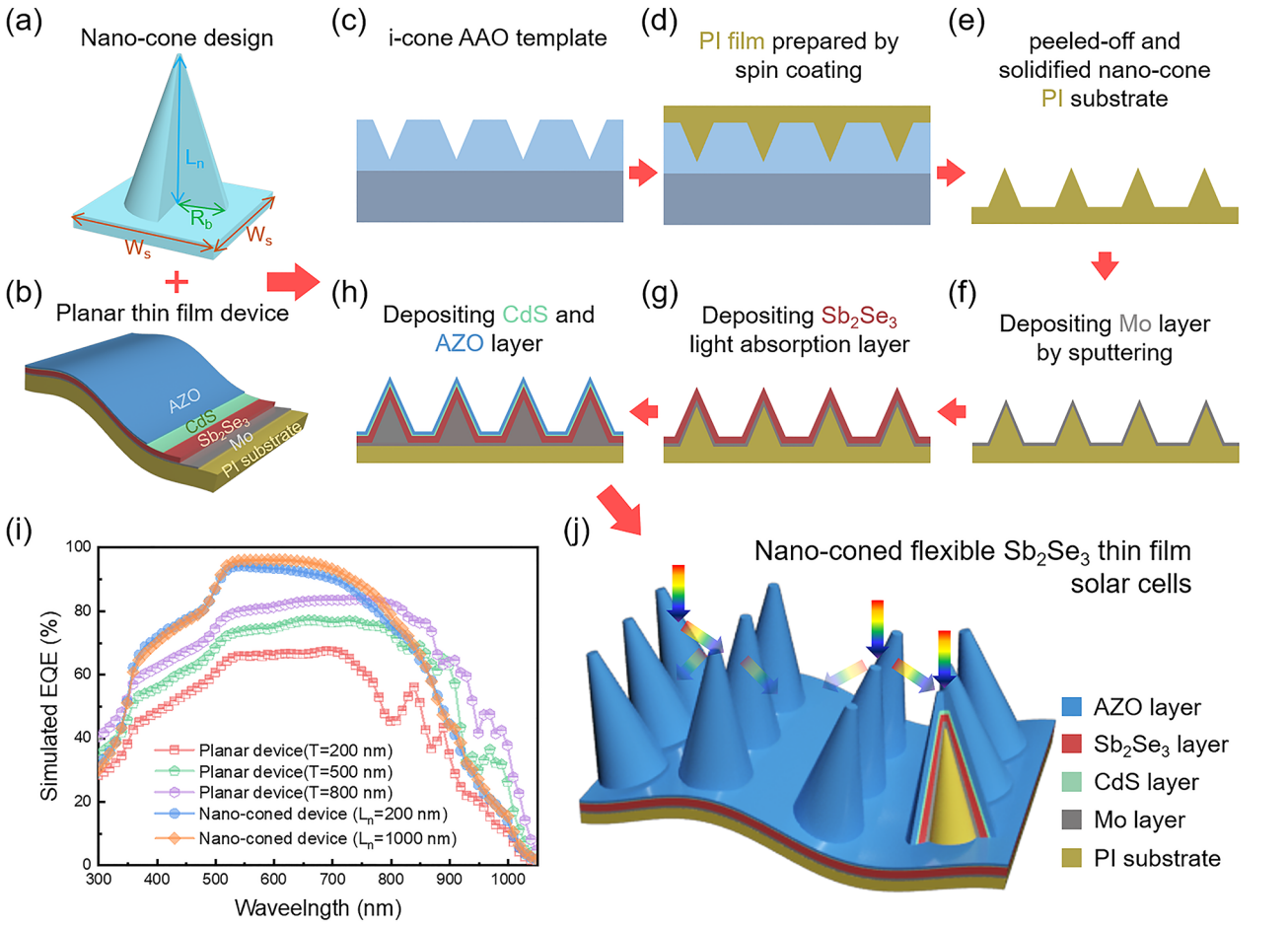


Figure 1. (a) Nanocone design, (b) planar Sb_2Se_3 thin film device, (c-h) fabrication procedures of nanoconed Sb_2Se_3 thin film solar cells, (i) EQE curves of the nanoconed and planar devices for comparison (W_s is 1800 nm, R_b is 500 nm), as well as (j) final-fabricated nanoconed Sb_2Se_3 units.

thin film devices, in terms of protecting the deposited thin film far away from the stress-rich region on the surface of the flexible substrate.[5,18−21] These vertically standing nanostructures can not only significantly enhance the robustness of the flexible thin film devices but also efficiently improve the light trapping capability to achieve a larger photocurrent, thus allowing the use of a very thin light absorption layer to help facilitate the carrier collection and tolerate more defective light absorption layer material.[5,22−25] More important, the carrier collection path and light absorption path can be decoupled, by reasonably designing/constructing the nanostructures.[18,26−28] However, these 3D nanostructures have never been introduced/constructed to fabricate high-performance and mechanically stale Sb_2Se_3-based flexible thin film solar cells, not to mention the investigation on their light absorption behaviors, especially under the back-reflection of the substrates.

In this work, we will first perform a straightforward comparison of the light-harvesting behavior of planar/nanoconed Sb_2Se_3 thin film solar cells on Mo-coated substrates based on a finite-element simulation to emphasize the benefit of light trapping effect realized among the 3D framework. Then, as shown in Figure 1a, we will investigate the evolutions of light absorption profiles under different lengths of the nanocone (L_n), bottom radius (R_b), aspect-ratios (L_n/R_b), and densities (represented by the width of the simulation box, W_s, as shown in Figure S1a), respectively, as well as the calculated external quantum efficiency (EQE) curves and integrated J_{sc}. Our results show that the reflection of the Mo layer deposited on the bottom surface of the substrates can help get an overall absorption enhancement during the full working wavelength range and weaken the role of the nanocone geometry on light harvesting behavior. However, whether the Mo layer deposited on the nanocone sidewall works positively or negatively on absorption enhancement, which arises from the resonant or scattering modes, is determined by the geometry of the nanoconed core. It is worth noting that this light absorption behavior has never been investigated and reported under the back-reflection of the substrates, and it is of practical importance for fabricating high-performance flexible optoelectronic thin film devices, especially on metal foil substrates that can be compliable with industry-mature roll-to-roll technology. Overall, this work can provide a practical guide to design/establish a simpler/easier fabrication process for constructing high-performance and mechanically stable flexible nanostructured Sb_2Se_3 thin film solar cells, which has never been reported before.

The device structure of nanoconed flexible Sb_2Se_3 thin film solar cells has been schematically drawn in Figure 1j, which presents a strong light trapping behavior among such a 3D nanostructure array. For a deeper understanding of the beneficial effect of such light trapping behavior, the simulated EQE curves of the planar Sb_2Se_3 thin film solar cells with thicknesses of 200, 500, and 800 nm, as well as the nanoconed

Downloaded from pubs.acs.org/jpclcd/article-pdf/15/38/9548/3360106/jz4c02414.pdf by NANJING UNIV user on 04 November 2026

https://doi.org/10.1021/acs.jpclett.4c02414
J. Phys. Chem. Lett. 2024, 15, 9548−9556

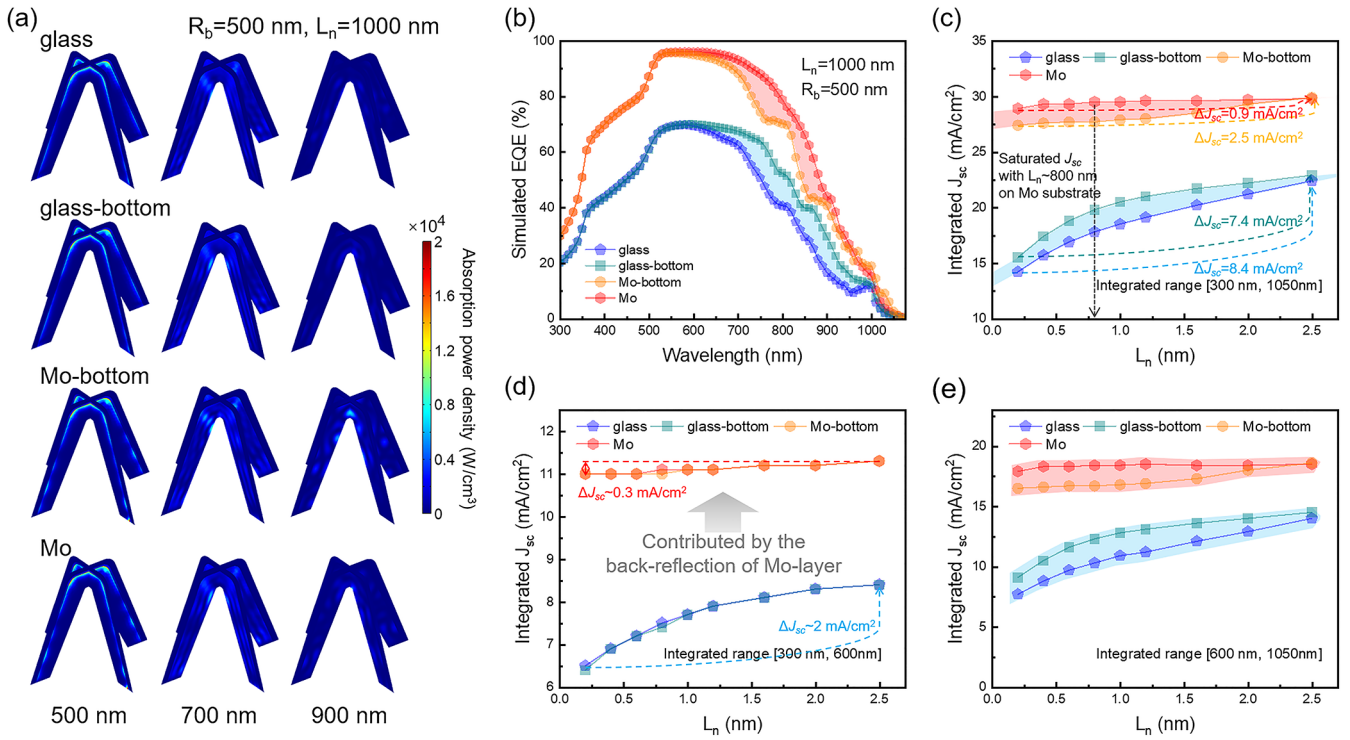


Figure 2. (a) Simulated light absorption profiles, and (b) simulated EQE curves of nanoconed Sb_2Se_3 units on glass, glass-bottom, Mo-bottom, Mo substrates, respectively (L_n is 1000 nm, R_b is 500 nm, W_s is 1800 nm). Integrated J_{sc} within the integrated range (c) [300 nm, 1050 nm], (d) [300 nm, 600 nm], (e) [600 nm, 1050 nm], as an evolution of different L_n values.

ones with L_n of 200 and 1000 nm, were calculated and presented in Figure 1i. The strong light trapping effect realized among the 3D nanostructures can enable sufficient light harvesting to allow the use of a very thin absorber (fixed at 200 nm in this work), which can help improve the light absorption material quality tolerance and thus address the electron diffusion length trade-off between [221] and [001] directions of Sb_2Se_3 thin film.[17] Furthermore, such 3D vertically standing nanostructures can host/support the subsequently deposited thin film to make the main working region out-of-plane.[5,17,29] In our previous work,[6,18] the simulated stress distribution of the radially stacked p-i-n junction, which was directly built upon the 3D vertical silicon nanowire framework grown by a vapor−liquid−solid (VLS) process, shows that the stresses at the top of the radial junction units are 3−4 orders of magnitude smaller than those found at the roots and on the nearby planar surface surrounding the radial junction units, indicating that the out-of-plane working regions can be well protected/kept away from the stress-rich bottom surface of the flexible substrate. All these results suggest that introducing nanostructures, such as nanocones and nanowires, as the core to host the subsequently deposited thin films can enable sufficient light harvesting and improve the mechanical stability for fabricating high-performance and robust flexible thin film solar cells. However, a fundamentally interesting, as well practically important, issue for building high-performance nanoconed Sb_2Se_3 thin film solar cells, which lies in that too long and too dense nanostructures would cause a nonuniform deposition of the thin film that results in nonuniform photocurrent generation among/or along the vertical standing units, should be well addressed. Thus, carrying out a profound investigation on light harvesting behavior, including the scattering and resonant modes, should be taken seriously to seek the best geometry and density design in the nanostructures, especially under the back-reflection of flexible metal foil substrate, which can be well compatible with the industrial-mature roll-to-roll technology, is meaningful and important.

Figures 2a and S4 show the simulated light absorption profiles, under different incident wavelengths from 300 to 1050 nm, extracted from normal-/cross-section surfaces of nanoconed Sb_2Se_3 units, with R_b of 500 nm, L_n of 1000 nm, and W_s of 1800 nm, on the four kinds of substrates, which are the following: *i*. the bottom and the nanocone parts without Mo coating (abbreviated as the glass substrate), *ii*. the bottom part without but the nanocone part with Mo coating (abbreviated as the glass-bottom substrate), *iii*. the bottom part with but the nanocone part without Mo coating (abbreviated as the Mo-bottom substrate), *iv*. the bottom and the nanocone parts with Mo coating (abbreviated as the Mo substrate), respectively. As seen from the simulated EQE curves of Sb_2Se_3 units on glass and Mo substrates plotted in Figure 2b, the back-reflection of the Mo substrates can greatly enhance light absorption during the full working wavelength range. Thus, the J_{sc} integrated from EQE values for the nanoconed Sb_2Se_3 units on the Mo substrates is much larger than that realized on the glass substrates, as shown in Figure 2c. Furthermore, as the L_n increases from 200 to 2500 nm, the J_{sc} shows a monotonously increasing trend on the glass substrate, from 14.2 mA/cm^2 to 22.4 mA/cm^2, while it first increases but then reaches a saturated value (29.5 mA/cm^2@L_n ~ 800 nm, and just with a ~0.9 mA/cm^2 improvement) when on the Mo substrate. With the contribution of the reflection of the Mo layer, the influence of increasing L_n, which can enhance the light trapping effect, on the EQE response values becomes less prominent. However, it should be pointed out that the Mo layer is

https://doi.org/10.1021/acs.jpclett.4c02414
J. Phys. Chem. Lett. 2024, 15, 9548−9556

Downloaded from pubs.acs.org/jpcicd/article-pdf/15/38/9548/3360106/jz4c02414.pdf by NANJING UNIV user on 04 November 2026

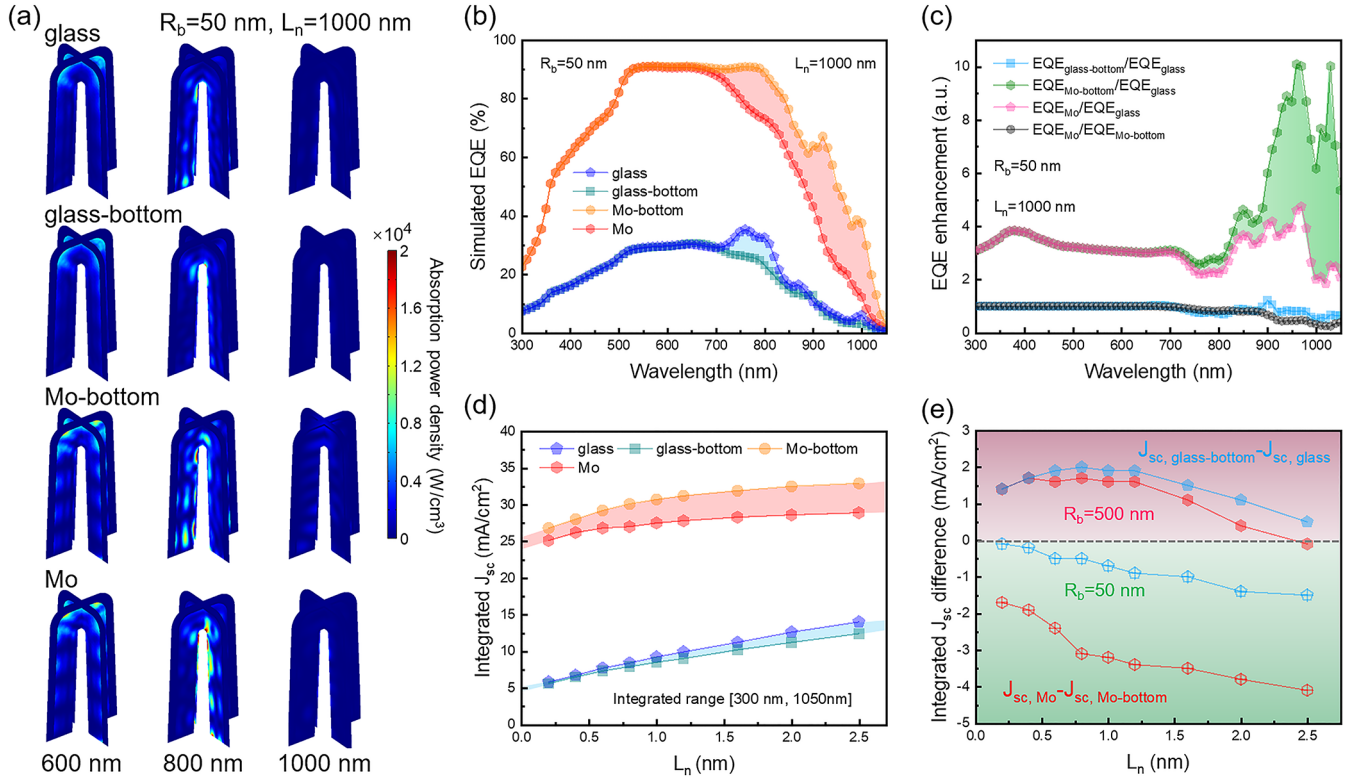


Figure 3. (a) Simulated light absorption profiles, (b) simulated EQE curves, and (c) EQE enhancement ratio of nanoconed Sb_2Se_3 units on glass, glass-bottom, Mo-bottom, Mo substrates, respectively (L_n is 1000 nm, R_b is 50 nm, W_s is 1800 nm). (d) Integrated J_{sc} within the integrated range [300 nm, 1050 nm], as an evolution of different L_n values, as well as (e) J_{sc} difference between Sb_2Se_3 units on Mo and Mo-bottom substrates, with R_b of 500 and 50 nm, respectively (blue solid pentagon: $J_{sc,\ glass\text{-}bottom}-J_{sc,\ glass}$, R_b = 500 nm; blue cross marked pentagon: $J_{sc,\ glass\text{-}bottom}-J_{sc,\ glass}$, R_b = 50 nm; red solid hexagon: $J_{sc,\ Mo}-J_{sc,\ Mo\text{-}bottom}$, R_b = 500 nm; red cross marked hexagon: $J_{sc,\ Mo}-J_{sc,\ Mo\text{-}bottom}$, R_b = 50 nm).

deposited not only on the bottom part but also on the sidewall part of the nanocones. How do the reflection of the bottom and nanocone sidewall parts work? The simulated EQE curves of the nanoconed Sb_2Se_3 units on glass-bottom and Mo-bottom substrates have also been presented in Figure 2b to highlight the beneficial effect of the 3D nanocones in light-harvesting behavior, as well as the integrated J_{sc} values in Figure 2c. As seen in Figure 2d, it is clear that the reflection of the Mo layer deposited on the sidewall of nanocones does not contribute to an obvious enhancement of the light absorption during the short wavelength (<600 nm) region. While switching to the long wavelength (>600 nm) region, the reflection of the Mo layer on the sidewall of nanocones positively works, as shown in Figure 2e, as well as the EQE enhancement ratio ($EQE_{Mo}/EQE_{Mo\text{-}bottom} > 1$ and $EQE_{glass\text{-}bottom}/EQE_{glass} > 1$) shown in Figure S7. Interestingly, as the L_n increases, the integrated J_{sc} differences in the full working wavelength range (between $J_{sc,\ Mo}$ and $J_{sc,\ Mo\text{-}bottom}$, or $J_{sc,\ glass\text{-}bottom}$ and $J_{sc,\ glass}$) becomes smaller, as shown in Figure 2c, which is inevitably related to the changed nanocone geometry.

Unexpectedly but reasonably, when changing the R_b value from 500 to 50 nm, a quite different situation of light response happens, as seen from the simulated light absorption profiles presented in Figures 3a and S9. Interestingly, compared to the ones on the glass-bottom (Mo) substrates, a much stronger light harvesting distribution can be observed for the nanoconed units on the glass (Mo-bottom) substrates during the long wavelength region (>600 nm), which is different from the light absorption behavior of the nanoconed units with R_b of 500 nm. Such results can be directly supported by the simulated EQE curves of Sb_2Se_3 units, as shown in Figures 3b and S11, as well as the EQE enhancement ratio values shown in Figures 3c and S12c–f, suggesting that during the long wavelength region (>600 nm), the values of $EQE_{Mo\text{-}bottom}$ (EQE_{glass}) are larger than EQE_{Mo} ($EQE_{glass\text{-}bottom}$), with the values of $EQE_{Mo}/EQE_{Mo\text{-}bottom}$ ($EQE_{glass\text{-}bottom}/EQE_{Glass}$) < 1. As shown in Figure 3d, with the L_n increasing from 200 to 2500 nm, the integrated J_{sc} values of the nanoconed Sb_2Se_3 units on the Mo (Mo-bottom) substrate increase from 25.1 mA/cm^2 (26.8 mA/cm^2) to 28.9 mA/cm^2 (32.9 mA/cm^2) with a saturated trend, while it on the glass (glass-bottom) substrate shows a nearly linear trend increasing from 5.8 mA/cm^2 (5.6 mA/cm^2) to 14 mA/cm^2 (12.4 mA/cm^2), respectively. More interesting, as the L_n increases from 200 to 2500 nm, the J_{sc} difference becomes larger, no matter whether between $J_{sc,\ Mo}$ and $J_{sc,\ Mo\text{-}bottom}$, or between $J_{sc,\ glass\text{-}bottom}$ and $J_{sc,\ glass}$, which is opposite to that of Sb_2Se_3 units with R_b of 500 nm. However, such J_{sc} difference is still mainly determined by the J_{sc} values integrated during long wavelength regions from 600 to 1050 nm, as shown in Figure S12a,b. Furthermore, the J_{sc} difference values between $J_{sc,\ Mo}$ and $J_{sc,\ Mo\text{-}bottom}$ ($J_{sc,\ Mo}-J_{sc,\ Mo\text{-}bottom}$, red solid hexagon for R_b = 500 nm, red cross marked hexagon for R_b = 50 nm), as well as $J_{sc,\ glass\text{-}bottom}$, and $J_{sc,\ glass}$ ($J_{sc,\ glass\text{-}bottom}-J_{sc,\ glass}$, blue solid hexagon for R_b = 500 nm, blue cross marked hexagon for R_b = 50 nm), have been calculated and plotted in Figure 3e, for the Sb_2Se_3 units with R_b of 500 or 50 nm, respectively, as a function of increasing L_n from 200 to 2500 nm. It is interesting to find that the most J_{sc} difference values for the Sb_2Se_3 units

https://doi.org/10.1021/acs.jpclett.4c02414
J. Phys. Chem. Lett. 2024, 15, 9548−9556

Downloaded from pubs.acs.org/jpclcd/article-pdf/15/38/9548/3360106/jz4c02414.pdf by NANJING UNIV user on 04 November 2026

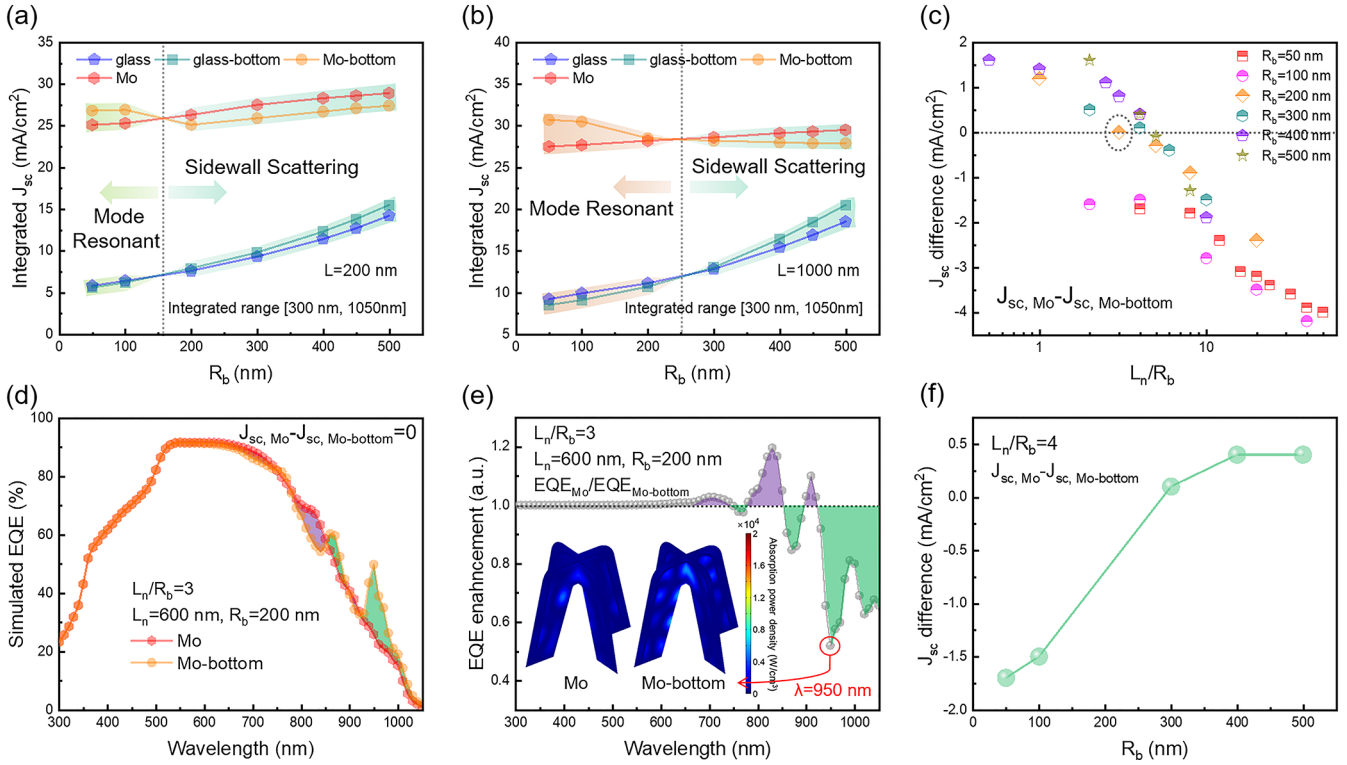


Figure 4. Integrated J_{sc} values for the Sb_2Se_3 units with (a) L_n = 200 nm and (b) L_n = 1000 nm, as a function of R_b, respectively. (c) J_{sc} difference values for nanoconed Sb_2Se_3 units as a function of L_n/R_b values. (d) Simulated EQE curves for the Sb_2Se_3 units on Mo and Mo-bottom substrates ($J_{sc, Mo}$−$J_{sc, Mo-bottom}$ = 0), and (e) corresponding EQE enhancement ratio (Inset: simulated light absorption profiles for the Sb_2Se_3 units on Mo/Mo-bottom substrates under the wavelength of 950 nm). (f) Calculated J_{sc} difference values for the Sb_2Se_3 units with L_n/R_b = 4, as a function of R_b values ranging from 50 to 500 nm.

with R_b of 500 nm, no matter whether $J_{sc, Mo}$−$J_{sc, Mo-bottom}$, or $J_{sc, glass-bottom}$−$J_{sc, glass}$ are larger than zero, except when the L_n increases to 2500 nm, the corresponding $J_{sc, Mo}$-$J_{sc, Mo-bottom}$ value is smaller than zero (−0.1 mA/cm^2). As R_b is 50 nm, all the J_{sc} difference values are smaller than zero. What can cause such interesting results? Indeed, among a 3D vertical-standing nanostructure array, as schematically drawn in Figure 1j, two different light absorption/interaction ways exist, which is *i*. the incident light is trapped and in-coupled into the resonant mode in a one-dimensional (1D) cavity-like nanostructure, following the concept of light injection into a fiber, or *ii*. the incident light scatters among 3D vertical-standing Sb_2Se_3 units and is harvested.[30−33]

To assess and distinguish the main contribution, which arises from the resonant or scattering modes in absorption enhancement, a simple but instructive simulation has been carried out by changing the R_b value from 50 to 500 nm (seems more like nanowire or nanocone), with L_n of 200 and 1000 nm, respectively. The J_{sc} values for the Sb_2Se_3 units on Mo and Mo-bottom substrates, with L_n values of 200 and 1000 nm, have been calculated by integrating the EQE response (Figure S13) and plotted as a function of R_b increasing from 50 to 500 nm, respectively, as shown in Figure 4a,b. As shown in Figure 4a (L_n ∼ 200 nm), with the R_b increasing from 50 to 500 nm, the integrated $J_{sc, Mo-bottom}$ decreases first, and then increases, but the $J_{sc, Mo}$ shows a monotonically increasing trend. More interestingly, when the R_b < ∼150 nm, the nanostructured core seems more like a 1D nanowire, and thus the $J_{sc, Mo-bottom}$ is larger than the $J_{sc, Mo}$, where the resonant mode works and plays a dominant role in absorption enhancement. However, when the R_b > ∼150 nm, the nanostructured core seems like the nanocone, and thus the $J_{sc, Mo-bottom}$ < $J_{sc, Mo}$, where the light scattering mode plays a determined role in the light-harvesting behavior, which can be supported by the simulated EQE curves plotted in Figure S14. When L_n = 1000 nm, as presented in Figure 4b, the integrated J_{sc} has a similar trend to that with L_n = 200 nm, except the turning point location is at ∼250 nm (R_b < ∼250 nm, $J_{sc, Mo-bottom}$ > $J_{sc, Mo}$; R_b > ∼250 nm, $J_{sc, Mo-bottom}$ < $J_{sc, Mo}$). As known, nanowire-based solar cells can directly benefit from the absorption enhancement induced by the resonant mode, which mainly depends on the geometric parameters of nanostructures.[33] Therefore, the geometric factor called aspect ratio, which can be defined by L_n/R_b, is introduced to describe the geometry of the nanostructure, as well as the J_{sc} difference values ($J_{sc, Mo}$−$J_{sc, Mo-bottom}$) have been calculated and plotted as a function of L_n/R_b in Figure 4c. Interestingly, when the R_b value is 50 or 100 nm, the J_{sc} difference values are always smaller than zero ($J_{sc, Mo-bottom}$ > $J_{sc, Mo}$), even the L_n is just 200 nm. However, when the R_b > 200 nm, the J_{sc} difference values decrease from positive to negative as the L_n/R_b increases, in other words, from $J_{sc, Mo}$ > $J_{sc, Mo-bottom}$ to $J_{sc, Mo}$ < $J_{sc, Mo-bottom}$. A small enough R_b or a large enough L_n makes a large enough L_n/R_b, which can help the nanostructured core seem more like a 1D nanowire, where the resonant mode plays a dominant role in absorption enhancement. Taking the $J_{sc, Mo}$-$J_{sc, Mo-bottom}$ = 0 for an example, as marked by a gray dash circle in Figure 4c, the L_n/R_b has a value of 3, with L_n = 600 nm, and R_b = 200 nm. From the simulated EQE curves presented in Figure 4d, it can be found that although the $J_{sc, Mo}$ = $J_{sc, Mo-bottom}$, the EQE curves of the Sb_2Se_3 units on Mo and Mo-bottom are similar but not identical, especially during the long-wavelength region,

Downloaded from pubs.acs.org/jpclcd/article-pdf/15/38/9548/3360106/jz4c02414.pdf by NANJING UNIV user on 04 November 2026

https://doi.org/10.1021/acs.jpclett.4c02414
J. Phys. Chem. Lett. 2024, 15, 9548−9556

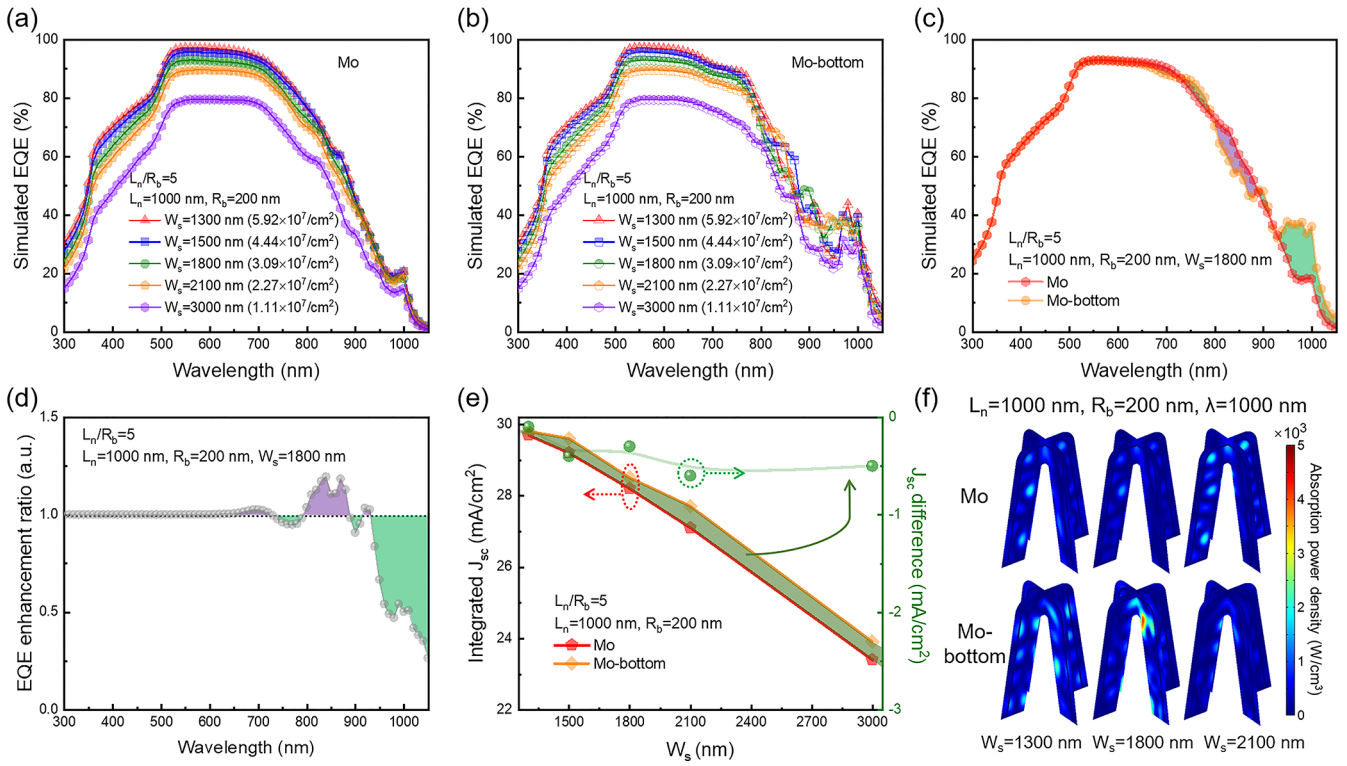


Figure 5. Simulated EQE curves for the nanoconed Sb_2Se_3 units on (a) Mo, and (b) Mo-bottom substrates, with different W_s values ranging from 1300 to 3000 nm (the corresponding density of nanoconed Sb_2Se_3 units is changed from $5.92 \times 10^7/cm^2$ to $1.11 \times 10^7/cm^2$), respectively. (c) Simulated EQE curves for the nanoconed Sb_2Se_3 units with $L_n/R_b = 5$, as well as (d) EQE enhancement ratio, (e) integrated J_{sc} values, and (f) extracted light absorption profiles, respectively (L_n = 1000 nm, R_b = 200 nm).

as well as the calculated EQE enhancement ratio ($EQE_{Mo}/EQE_{Mo\text{-}bottom}$) values as a function of the wavelengths plotted in Figure 4e. Furthermore, the light absorption profiles have been extracted under λ = 950 nm and presented as an inset in Figure 4e, to get a deeper insight into such an interesting light-harvesting behavior. The light absorption profile, extracted from the sample on the Mo-bottom substrate, shows a more effective light harvesting within the absorber layer with relatively uniform power distribution, compared to the one on the Mo substrate, which just has the highest absorption zones near the top segment of the core. This phenomenon indicates that the incident light has been coupled/collected effectively into the nanowire-like structure, following the field distributions of the resonant propagating modes within the 1D cavity,[30,33] for the nanoconed Sb_2Se_3 units on the Mo-bottom substrate. At the same time, the Mo layer on the sidewall of nanocones reflects the incident light and prevents a deeper propagation into the absorber layer. Besides, as shown in Figure 4f, the J_{sc} difference values ($J_{sc,\,Mo} - J_{sc,\,Mo\text{-}bottom}$) for the Sb_2Se_3 units with L_n/R_b = 4, have been calculated and plotted as a function of increasing R_b, as well as the calculated EQE enhancement ratio and the simulated light absorption profiles at the long wavelength region (Figure S18). The J_{sc} difference values show a monotonically increasing trend, changing from negative to positive (from $J_{sc,\,Mo} < J_{sc,\,Mo\text{-}bottom}$ to $J_{sc,\,Mo} > J_{sc,\,Mo\text{-}bottom}$), indicating that a larger R_b needs a larger L_n/R_b to help the resonant mode play a dominant role in absorption enhancement, in other words, a large enough length L_n is needed to make the nanostructured core seem like 1D nanowire cavity. For example, as shown in Figure S19, even if the R_b is 500 nm, when the L_n is 3000 or 4000 nm, the $J_{sc,\,Mo} - J_{sc,\,Mo\text{-}bottom}$, and $J_{sc,\,glass\text{-}bottom} - J_{sc,\,glass}$ values are smaller than zero.

Another important geometry parameter is the density of the nanoconed Sb_2Se_3 units, which has been proven to play an important role in the absorption enhancement of such 3D nanostructures.[34,35] The simulations for the nanoconed Sb_2Se_3 units with different densities can be performed by changing the simulation box width (W_s), as defined in Figure S1a, from 1300 to 3000 nm, with the corresponding density changing from $5.92 \times 10^7/cm^2$ to $1.11 \times 10^7/cm^2$, respectively. The simulated EQE curves of the nanoconed Sb_2Se_3 units on the Mo and Mo-bottom substrates have been plotted in Figure 5a and b, respectively, as well as the light absorption profiles in Figure S20. As the W_s increases, the EQE curves, whether on the Mo or Mo-bottom substrates, decline obviously in the full working wavelength range. The decreased EQE curves are similar but not identical, especially during the long wavelength region >900 nm. The EQE curves on the Mo-bottom substrates have a stronger absorption peak at λ = 900 nm, compared to that on the Mo substrates, which can be seen more clearly from the EQE curves plotted in Figure 5c, for the nanoconed Sb_2Se_3 units with L_n = 1000 nm, R_b = 200 nm, and W_s = 1800 nm. Also, the EQE enhancement ratio has been calculated and plotted in Figure 5d, showing that when the λ > 900 nm, $EQE_{Mo}/EQE_{Mo\text{-}bottom} < 1$, which can also be supported by the extracted absorption profiles shown in Figure 5f. A similar phenomenon can be observed with other W_s values, as shown in Figure S21. The integrated J_{sc} values are shown in Figure 5e, as a function of W_s, as well as the calculated J_{sc} difference. When changing the W_s from 1300 to 3000 nm, both the integrated J_{sc} show a monotonically decreasing trend, with a decline of −6.3 mA/cm^2 for the

https://doi.org/10.1021/acs.jpclett.4c02414
J. Phys. Chem. Lett. 2024, 15, 9548−9556

Downloaded from pubs.acs.org/jpclcd/article-pdf/15/38/9548/3360106/jz4c02414.pdf by NANJING UNIV user on 04 November 2026

Sb_2Se_3 units on the Mo substrates (from 29.7 mA/cm^2 to 23.4 mA/cm^2), and −5.9 mA/cm^2 for the Mo-bottom substrates (from 29.8 mA/cm^2 to 23.9 mA/cm^2). Thus, the J_{sc} difference changes from −0.1 to −0.5 mA/cm^2, as shown in Figure 5e. A similar varied trend also happens for the nanoconed Sb_2Se_3 units with L_n = 600 nm, and R_b = 200 nm, as shown in Figure S22.

All these observations indicate that *i*. the back-reflection of the Mo layer deposited on the bottom part of the substrate can help get an overall absorption enhancement within the absorber; *ii*. with the back-reflection of the Mo layer, the absorption enhancement is still affected by the geometry of nanoconed cores, especially during the long wavelength region, but this function has been weakened compared to that on the glass substrates; *iii*. when the nanoconed core seems like a 1D nanowire cavity, the absorption enhancement is dominated by the resonant mode, and the Mo layer on the nanocone sidewall would prevent a deeper light propagation into the nanoconed Sb_2Se_3 unit; *iv*. When the light scattering mode dominates the absorption enhancement, the reflection of the Mo layer deposited on the nanocone sidewall can help the effective light path be much larger than the physical diameter.

In summary, this work is the first demonstration to investigate the light absorption behavior for the nanostructured thin film solar cells under the back-reflection of the substrates, especially the reflection from the nanostructure sidewall. By performing simulations of the nanoconed Sb_2Se_3 unit on the glass, glass-bottom, Mo-bottom, and Mo substrates, the light absorption profiles under different geometries have been investigated, which shows that the light-harvesting can be enhanced by the back-reflection of the Mo layer deposited on the bottom surface of the substrates; however, the effect of sidewall Mo layer on absorption enhancement, arising from resonant or scattering modes, is determined by the geometry of the nanocone. These results have provided a unique perspective guide in designing the nanostructure for thin film solar cells and establishing an easier and simpler process to fabricate high-performance and mechanically stable flexible nanostructured Sb_2Se_3 thin film solar cells, which has never been reported before.

METHODOLOGY

Simulation Model. The design and fabrication process of flexible nanostructured Sb_2Se_3 thin film solar cells has been shown schematically in Figure 1a to 1h. According to the published literature on planar thin film devices,[14] the simulation model is built, as shown in Figure S1a,b. Taking the geometrical dimensions (L_n, R_b, W_s) of the nanocone into consideration, as well as fixing the top radius of the nanocone at 2.5 nm and thickness of the light absorption layer at 200 nm, a finite-element simulation has been carried out on the light absorption behavior, within a periodic array of nanoconed Sb_2Se_3 thin film units on the glass substrate with/without Mo coating (*i*. the glass substrate, *ii*. the glass-bottom substrate, *iii*. the Mo-bottom substrate, *iv*. the Mo substrate), as schematically drawn in Figure S1c−f. The complex refractive index (n-k) curves of Mo, CdS, Sb_2Se_3, and AZO layers in this simulation, extracted from published literature,[36−38] are shown in Figure S2. Besides, for a simplified representation, the bottom planar part among the nanoconed units has been removed in all performed simulations in this work, which can help us focus on the contribution arising from nanocones.

Optical Calculation. Using the following equation, the absorption power distribution (P_{abs}) can be calculated

$$P_{abs} = c \cdot I_{in} \cdot 4\pi k/\lambda$$

where c is the light speed in vacuum, $I_{in} = \varepsilon E^2/2$ is the local electromagnetic energy density, k is the imaginary part of the refractive index $\tilde{n} = n + ik$.

Then, the percentage of effective absorption realized in the Sb_2Se_3 absorber can be calculated by integrating the power dissipation losses within a selected volume of each material layer, and normalizing them with respect to the total power of the incident light field, as following

$$W_{Sb_2Se_3} = \int_{Sb_2Se_3 layer} P_{abs} dv / P_{incident}$$

where $P_{incident} = \int_{top\text{-}plane} \frac{1}{2} c \cdot \varepsilon \cdot E^2 ds$

The effective absorption power can correspond to an upper bound of the EQE of the thin film solar cells (excluding recombination issues), when assuming that the absorption of one photon generates only one electron−hole pair.

Then, the short-circuit photocurrent density (J_{sc}) can be calculated by

$$J_{sc,EQE} = \int qEQE(\lambda)S(\lambda)d\lambda$$

where $S(\lambda)$ is photons per second.

ASSOCIATED CONTENT

Supporting Information

The Supporting Information is available free of charge at https://pubs.acs.org/doi/10.1021/acs.jpclett.4c02414.

Built geometry of a single nanoconed Sb_2Se_3 unit in a cubic box for the finite-element simulation. Complex refractive index (n-k) curves for Mo, Sb_2Se_3, CdS, and AZO layers in this simulation. Simulated light absorption profiles, calculate EQE curves as well as EQE enhancement ratio, and integrated J_{sc} values (PDF)

AUTHOR INFORMATION

Corresponding Authors

Shaobo Zhang − *College of Physical Science and Technology/Microelectronics Industry Research Institute, Yangzhou University, 225002 Yangzhou, P. R. China; School of Electronics Science and Engineering/National Laboratory of Solid State Microstructures, Nanjing University, 210023 Nanjing, P. R. China;* orcid.org/0000-0001-7597-3462; Email: shaobozhang@yzu.edu.cn

Ruijin Hu − *College of Physical Science and Technology/Microelectronics Industry Research Institute, Yangzhou University, 225002 Yangzhou, P. R. China; School of Electronics Science and Engineering/National Laboratory of Solid State Microstructures, Nanjing University, 210023 Nanjing, P. R. China;* orcid.org/0009-0006-5973-6954; Email: huruijin@yzu.edu.cn

Linwei Yu − *School of Electronics Science and Engineering/National Laboratory of Solid State Microstructures, Nanjing University, 210023 Nanjing, P. R. China;* orcid.org/0000-0002-0801-5210; Email: yulinwei@nju.edu.cn

Downloaded from pubs.acs.org/jpclcd/article-pdf/15/38/9548/3360106/jz4c02414.pdf by NANJING UNIV user on 04 November 2026

https://doi.org/10.1021/acs.jpclett.4c02414
J. Phys. Chem. Lett. 2024, 15, 9548−9556

Authors

Cheng Chen − *College of Physical Science and Technology/Microelectronics Industry Research Institute, Yangzhou University, 225002 Yangzhou, P. R. China*

Yunqing Cao − *College of Physical Science and Technology/Microelectronics Industry Research Institute, Yangzhou University, 225002 Yangzhou, P. R. China*

Xiangdong Meng − *College of Physical Science and Technology/Microelectronics Industry Research Institute, Yangzhou University, 225002 Yangzhou, P. R. China*

Zongguang Liu − *College of Physical Science and Technology/Microelectronics Industry Research Institute, Yangzhou University, 225002 Yangzhou, P. R. China;* orcid.org/0000-0003-4141-7462

Haifeng Gao − *Cell R&D Center, JA Solar Holdings Co. Ltd, Yangzhou 225000, P. R. China*

Xiulin Jiang − *Cell R&D Center, JA Solar Holdings Co. Ltd, Yangzhou 225000, P. R. China*

Junzhuan Wang − *School of Electronics Science and Engineering/National Laboratory of Solid State Microstructures, Nanjing University, 210023 Nanjing, P. R. China*

Complete contact information is available at: https://pubs.acs.org/10.1021/acs.jpclett.4c02414

Notes

The authors declare no competing financial interest.

■ ACKNOWLEDGMENTS

The authors acknowledged the financial supports from the Special Fund for City School Cooperation of Yangzhou City (No. YZ2022177), Innovation technology platform project jointly built by Yangzhou City and Yangzhou University (No. YZ2020268), Natural Science Foundation of Jiangsu Province (No. BK20230562), National Natural Science Foundation of China under No. 61974064, 62304200, 61934004, National Natural Science Foundation of China for Distinguished Young Scholars No. 62325403, and National Key Research Program of China under Grant No. 92164201.

■ REFERENCES

(1) Park, S.; Heo, S. W.; Lee, W.; Inoue, D.; Jiang, Z.; Yu, K.; Jinno, H.; Hashizume, D.; Sekino, M.; Yokota, T.; Fukuda, K.; Tajima, K.; Someya, T. Self-powered ultra-flexible electronics via nano-grating-patterned organic photovoltaics. *Nature* **2018**, *561*, 516−521.

(2) Dai, H.; Yang, L.; He, S. <50-μm thin crystalline silicon heterojunction solar cells with dopant-free carrier-selective contacts. *Nano Energy* **2019**, *64*, No. 103930.

(3) Chen, C.; Li, K.; Li, F.; Wu, B.; Jiang, P.; Wu, H.; Lu, S.; Tu, G.; Liu, Z.; Tang, J. One-Dimensional Sb2Se3 Enabling a Highly Flexible Photodiode for Light-Source-Free Heart Rate Detection. *ACS Photonics* **2020**, *7*, 352−360.

(4) Zhang, S.; Zhang, T.; Liu, Z.; Wang, J.; Yu, L.; Xu, J.; Chen, K.; Roca i Cabarrocas, P. Highly flexible radial tandem junction thin film solar cells with excellent power-to-weight ratio. *Nano Energy* **2021**, *86*, No. 106121.

(5) Lin, Q.; Lu, L.; Tavakoli, M. M.; Zhang, C.; Lui, G. C.; Chen, Z.; Chen, X.; Tang, L.; Zhang, D.; Lin, Y.; Chang, P.; Li, D.; Fan, Z. High performance thin film solar cells on plastic substrates with nanostructure-enhanced flexibility. *Nano Energy* **2016**, *22*, 539−547.

(6) Zhang, S.; Zhang, T.; Liu, Z.; Wang, J.; Xu, J.; Chen, K.; Yu, L. Flexible and Robust 3D a-SiGe Radial Junction Near-Infrared Photodetectors for Rapid Sphygmic Signal Monitoring. *Adv. Funct. Mater.* **2022**, *32*, No. 2107040.

(7) Mavlonov, A.; Razykov, T.; Raziq, F.; Gan, J.; Chantana, J.; Kawano, Y.; Nishimura, T.; Wei, H.; Zakutayev, A.; Minemoto, T.; Zu, X.; Li, S.; Qiao, L. A review of Sb2Se3 photovoltaic absorber materials and thin-film solar cells. *Sol. Energy* **2020**, *201*, 227−246.

(8) Wang, X.; Kavanagh, S. R.; Scanlon, D. O.; Walsh, A. Upper efficiency limit of Sb2Se3 solar cells. *Joule* **2024**, *8* (7), 2105−2122.

(9) Shongalova, A.; Correia, M. R.; Teixeira, J. P.; Leitão, J. P.; González, J. C.; Ranjbar, S.; Garud, S.; Vermang, B.; Cunha, J. M. V.; Salomé, P. M. P.; Fernandes, P. A. Growth of Sb2Se3 thin films by selenization of RF sputtered binary precursors. *Sol. Energy Mater. Sol. Cells* **2018**, *187*, 219−226.

(10) Zhou, Y.; Wang, L.; Chen, S.; Qin, S.; Liu, X.; Chen, J.; Xue, D.-J.; Luo, M.; Cao, Y.; Cheng, Y.; Sargent, E. H.; Tang, J. Thin-film Sb2Se3 photovoltaics with oriented one-dimensional ribbons and benign grain boundaries. *Nat. Photonics* **2015**, *9* (6), 409−415.

(11) Wang, L.; Li, D.-B.; Li, K.; Chen, C.; Deng, H.-X.; Gao, L.; Zhao, Y.; Jiang, F.; Li, L.; Huang, F.; He, Y.; Song, H.; Niu, G.; Tang, J. Stable 6%-efficient Sb2Se3 solar cells with a ZnO buffer layer. *Nat. Energy* **2017**, *2* (4), No. 17046.

(12) Chen, S.; Ye, Y. A.; Ishaq, M.; Ren, D. L.; Luo, P.; Wu, K. W.; Zeng, Y. J.; Zheng, Z. H.; Su, Z. H.; Liang, G. X. Simultaneous Band Alignment Modulation and Carrier Dynamics Optimization Enable Highest Efficiency in Cd-Free Sb2Se3 Solar Cells. *Adv. Funct. Mater.* **2024**, No. 2403934.

(13) Duan, Z.; Liang, X.; Feng, Y.; Ma, H.; Liang, B.; Wang, Y.; Luo, S.; Wang, S.; Schropp, R. E. I.; Mai, Y.; Li, Z. Sb2Se3 Thin-Film Solar Cells Exceeding 10% Power Conversion Efficiency Enabled by Injection Vapor Deposition Technology. *Adv. Mater.* **2022**, *34* (30), No. 2202969.

(14) Liang, X.; Feng, Y.; Dang, W.; Huang, H.; Wang, X.; Guo, Y.; Shen, K.; Schropp, R. E. I.; Li, Z.; Mai, Y. High-Efficiency Flexible Sb2Se3 Solar Cells by Back Interface and Absorber Bulk Deep-Level Trap Engineering. *ACS Energy Lett.* **2023**, *8* (1), 213−221.

(15) Tang, R.; Wang, X.; Lian, W.; Huang, J.; Wei, Q.; Huang, M.; Yin, Y.; Jiang, C.; Yang, S.; Xing, G.; Chen, S.; Zhu, C.; Hao, X.; Green, M. A.; Chen, T. Hydrothermal deposition of antimony selenosulfide thin films enables solar cells with 10% efficiency. *Nat. Energy* **2020**, *5* (8), 587−595.

(16) Wen, X.; Lu, Z.; Wang, G.-C.; Washington, M. A.; Lu, T.-M. Efficient and stable flexible Sb2Se3 thin film solar cells enabled by an epitaxial CdS buffer layer. *Nano Energy* **2021**, *85*, No. 106019.

(17) Li, Z.; Liang, X.; Li, G.; Liu, H.; Zhang, H.; Guo, J.; Chen, J.; Shen, K.; San, X.; Yu, W.; Schropp, R. E. I.; Mai, Y. 9.2%-efficient core-shell structured antimony selenide nanorod array solar cells. *Nat. Commun.* **2019**, *10* (1), 125.

(18) Wang, S.; Zhang, S.; Liu, Z.; Wang, J.; Xu, J.; Yu, L. High-performance radial junction solar cells on ZnO coated stainless steel with excellent flexibility and durability. *Nano Energy* **2024**, *122*, No. 109262.

(19) Zhang, S.; Yu, L. 3D Radial Junctions for Robust and Flexible Optoelectronics. *Advanced Optical Materials* **2024**, *12* (9), No. 2302121.

(20) Prajapati, A.; Nissan, Y.; Gabay, T.; Shalev, G. Broadband absorption of the solar radiation with surface arrays of subwavelength light funnels. *Nano Energy* **2018**, *54*, 447−452.

(21) Dong, W. J.; Yoo, C. J.; Cho, H. W.; Kim, K.-B.; Kim, M.; Lee, J.-L. Flexible a-Si:H Solar Cells with Spontaneously Formed Parabolic Nanostructures on a Hexagonal-Pyramid Refl ector. *small* **2015**, *11* (16), 1947−1953.

(22) Lu, Y.; Lal, A. High-efficiency ordered silicon nano-conical-frustum array solar cells by self-powered parallel electron lithography. *Nano Lett.* **2010**, *10* (11), 4651−4656.

(23) Pathirane, M. K.; Wong, W. S. Optical and Electrical Characteristics of Hybrid ZnO Nanowire/a-Si:H Solar Cells on Flexible Substrates under Mechanical Bending. *Small* **2016**, *12* (19), 2554−2558.

(24) Kwon, J. Y.; Lee, D. H.; Chitambar, M.; Maldonado, S.; Tuteja, A.; Boukai, A. High efficiency thin upgraded metallurgical-grade

Downloaded from pubs.acs.org/jpclcd/article-pdf/15/38/9548/3360106/jz4c02414.pdf by NANJING UNIV user on 04 November 2026

silicon solar cells on flexible substrates. *Nano Lett.* **2012**, *12* (10), 5143−5147.
(25) Zhang, S.; Zhang, T.; Cao, L.; Liu, Z.; Wang, J.; Xu, J.; Chen, K.; Yu, L. Coupled boron-doping and geometry control of tin-catalyzed silicon nanowires for high performance radial junction photovoltaics. *Opt. Express* **2019**, *27* (26), 37248−37256.
(26) Tian, B.; Zheng, X.; Kempa, T. J.; Fang, Y.; Yu, N.; Yu, G.; Huang, J.; Lieber, C. M. Coaxial silicon nanowires as solar cells and nanoelectronic power sources. *Nature* **2007**, *449* (7164), 885−889.
(27) Tang, J.; Huo, Z.; Brittman, S.; Gao, H.; Yang, P. Solution-processed core-shell nanowires for efficient photovoltaic cells. *Nature Nanotechnol.* **2011**, *6* (9), 568−572.
(28) Mohite, A. D.; Perea, D. E.; Singh, S.; Dayeh, S. A.; Campbell, I. H.; Picraux, S. T.; Htoon, H. Highly efficient charge separation and collection across in situ doped axial VLS-grown Si nanowire p−n junctions. *Nano Lett.* **2012**, *12* (4), 1965−1971.
(29) Dong, W. J.; Yoo, C. J.; Cho, H. W.; Kim, K.-B.; Kim, M.; Lee, J.-L. Flexible a-Si:H Solar Cells with Spontaneously Formed Parabolic Nanostructures on a Hexagonal-Pyramid Refl ector. *Small* **2015**, *11* (16), 1947−1953.
(30) Lu, J.; Qian, S.; Yu, Z.; Misra, S.; Yu, L.; Xu, J.; Shi, Y.; Roca i Cabarrocas, P.; Chen, K. How tilting and cavity-mode-resonant absorption contribute to light harvesting in 3D radial junction solar cells. *Opt. Express* **2015**, *23* (19), A1288−1296.
(31) Zhang, S.; Wang, S.; Hu, R.; Cao, Y.; Wang, J.; Xu, J.; Yu, L. How backreflection contributes to light absorption for high-performance radial junction photovoltaics. *Appl. Phys. Lett.* **2023**, *123* (23), No. 231102.
(32) Kelzenberg, M. D.; Boettcher, S. W.; Petykiewicz, J. A.; Turner-Evans, D. B.; Putnam, M. C.; Warren, E. L.; Spurgeon, J. M.; Briggs, R. M.; Lewis, N. S.; Atwater, H. A. Enhanced absorption and carrier collection in Si wire arrays for photovoltaic applications. *Nature materials* **2010**, *9* (3), 239−244.
(33) Cao, L.; White, J. S.; Park, J. S.; Schuller, J. A.; Clemens, B. M.; Brongersma, M. L. Engineering light absorption in semiconductor nanowire devices. *Nature materials* **2009**, *8* (8), 643−647.
(34) Misra, S.; Yu, L.; Foldyna, M.; Roca i Cabarrocas, P. High efficiency and stable hydrogenated amorphous silicon radial junction solar cells built on VLS-grown silicon nanowires. *Sol. Energy Mater. Sol. Cells* **2013**, *118*, 90−95.
(35) Li, Y.; Chen, Q.; He, D.; Li, J. Radial junction Si micro/nanowire array photovoltaics: Recent progress from theoretical investigation to experimental realization. *Nano Energy* **2014**, *7*, 10−24.
(36) Werner, W. S. M.; Glantschnig, K.; Ambrosch-Draxl, C. Optical Constants and Inelastic Electron-Scattering Data for 17 Elemental Metals. *J. Phys. Chem. Ref. Data* **2009**, *38* (4), 1013−1092.
(37) Treharne, R. E.; Seymour-Pierce, A.; Durose, K.; Hutchings, K.; Roncallo, S.; Lane, D. Optical Design and Fabrication of Fully Sputtered CdTe/CdS Solar Cells. *J. Phys. Conf. Ser.* **2011**, *286*, No. 012038.
(38) Chen, C.; Li, W.; Zhou, Y.; Chen, C.; Luo, M.; Liu, X.; Zeng, K.; Yang, B.; Zhang, C.; Han, J.; Tang, J. Optical properties of amorphous and polycrystalline Sb2Se3 thin films prepared by thermal evaporation. *Appl. Phys. Lett.* **2015**, *107* (4), No. 043905.

Downloaded from pubs.acs.org/jpclcd/article-pdf/15/38/9548/3360106/jz4c02414.pdf by NANJING UNIV user on 04 November 2026

https://doi.org/10.1021/acs.jpclett.4c02414
J. Phys. Chem. Lett. 2024, 15, 9548−9556